Acta Biochim Biophys Sin 2026, 58(6): 1387–1401
https://cstr.cn/32197.14.abbs.2025139
https://doi.org/10.3724/abbs.2025139
Original Article

Original Article

Angelicin attenuates sepsis-associated acute liver injury via p38 MAPK inhibition and NF-κB-mediated Nrf2/Keap1 activation to suppress inflammation and oxidative stress

Enzhuang Pan[1,†], Huilin Sun[2,†], Shasha Zhang[1], Jun Wang[1], Yedan Liu[1], Feibiao Wang[1], Jing Xia[1], Yingjia Qian[1], Xiaolong Xu[3,*], and Jingquan Dong[1,*]

[1]Jiangsu Marine Pharmaceutical Resources Development Engineering Research Center, Jiangsu Key Laboratory of Marine Pharmaceutical Compound Screening, College of Pharmacy, Jiangsu Ocean University, Lianyungang 222005, China, [2]School of Medicine, Nantong University Xinglin College, Nantong 226236, China, and [3]Department of Pharmacy, Lianyungang Affiliated Hospital of Nanjing University of Chinese Medicine, Lianyungang 222004, China

[†]These authors contributed equally to this work.

*Correspondence address. E-mail: xuxiaolong1124@yeah.net (X.X.); 2018000029@jou.edu.cn (J.D.)

Received 18 April 2025 Accepted 28 July 2025 Published 28 October 2025

Abstract

Sepsis-associated acute liver injury (SALI) is a frequent and clinically severe complication of sepsis, in which inflammatory responses and oxidative stress are involved. Angelicin (ANG), one of the main active components in the traditional Chinese medicine *Psoralea corylifolia* Linn., has anti-inflammatory and antioxidant bioactivities. In this study, the protective effect of ANG on SALI and its specific mechanism are investigated by establishing a mouse model of caecal ligation and puncture (CLP)-induced SALI and an *in vitro* sepsis model in LPS-stimulated AML12 cells. These results show that ANG can alleviate liver injury and improve liver function in SALI mice. ANG decreases the mRNA expression levels of the pro-inflammatory factors *Il-1β*, *Il-6*, and *Tnf-α* and increases the mRNA expression level of the anti-inflammatory factor *Il-10*, which suggests its anti-inflammatory effects. The results of the biochemical kit assay and DHE staining show that ANG can decrease the levels of MDA and ROS and increase the level of GSH and the activities of CAT and SOD, which suggests that ANG has antioxidant effects. Mechanistically, ANG exerts anti-inflammatory effects by inhibiting the NF-κB and p38 MAPK pathways and exerting antioxidant effects by activating the Nrf2/Keap1 pathway. Additionally, cell transfection experiments indicate that activation of the Nrf2/Keap1 pathway by ANG may depend on the inhibition of the NF-κB pathway. In conclusion, ANG attenuates SALI by inhibiting the NF-κB and p38 MAPK pathways, thereby activating the Nrf2/Keap1 pathway and making it a promising therapeutic intervention for SALI.

Key words angelicin, sepsis-associated acute liver injury, inflammation, oxidative stress

Introduction

Sepsis is a systemic inflammatory response caused by infection, and when this inflammatory response is out of control, it may lead to damage to multiple organ systems [1]. The liver is a key effector in sepsis pathogenesis, orchestrating host defense via microbial antigen clearance, immune cell recruitment, and inflammation-associated metabolic shifts, thereby frequently becoming a major affected organ [2]. Sepsis not only causes acute liver injury, leading to liver failure but also may lead to serious complications, such as biliary obstruction, hepatic encephalopathy, and multiple organ dysfunction syndrome (MODS) [2]. However, few studies have investigated sepsis-associated acute liver injury (SALI).

Recent investigations revealed that physiological responses, including oxidative stress, inflammatory signaling, and programmed cell death (apoptosis), play essential protective roles against SALI [3]. However, excessive activation of these pathways paradoxically aggravates tissue damage *in vivo* [4]. As heterologous phagocytes in innate immunity, macrophages detect pathogen-

© The Author(s) 2025. This is an open access article distributed under the terms of the Creative Commons Attribution License (https://creativecommons.org/licenses/by/4.0/).

associated molecular patterns (PAMPs) and damage-associated molecular patterns (DAMPs) by expressing pattern-recognition receptors [5]. During sepsis pathogenesis, hepatic non-parenchymal cells, including Kupffer cells, hepatic sinusoidal endothelial cells, and stellate cells, serve as the primary defense mechanism by capturing and eliminating invading pathogenic microorganisms and their byproducts, thereby providing systemic protection while maintaining hepatic homeostasis [6]. Moreover, liver-resident and recruited immune cells produce multiple proinflammatory cytokines and chemokines that lead to liver injury and dysfunction during sepsis [7]. Liver dysfunction has been demonstrated to be a distinct and independent predictor of adverse outcomes in critically ill patients [8], whereas pre-existing hepatic impairment predisposes individuals to sepsis, subsequent multi-organ failure, and increased mortality. Therefore, anti-inflammatory interventions that mitigate liver injury and restore hepatic function could improve outcomes in sepsis patients [9].

Extensive evidence indicates that various signaling pathways, particularly the mitogen-activated protein kinase (MAPK) and nuclear factor-κB (NF-κB) pathways, critically regulate inflammatory responses during sepsis pathogenesis [10]. The MAPK family, which comprises extracellular signal-regulated kinases 1/2 (ERK1/2), p38 mitogen-activated protein kinase (p38 MAPK), and c-Jun N-terminal kinase (JNK), modulates the transcriptional regulation of proinflammatory mediators, including inducible nitric oxide synthase (iNOS) and cyclooxygenase-2 (COX-2). Moreover, NF-κB, a heterodimer of p50/p65 subunits that complex with inhibitory κB (IκB) proteins, plays a bidirectional role in both host defense mechanisms and the orchestration of proinflammatory cytokine production and release. Thus, inhibition of the MAPK and NF-κB signaling pathways could contribute to reducing inflammation to ameliorate SALI.

Oxidative stress is recognized as a pivotal contributor to sepsis progression, and its pathophysiological mechanisms are intimately implicated in pathogenesis [3]. During sepsis, excessive production of reactive oxygen species (ROS) and the resulting lipid peroxidation cascade constitute a major pathogenic mechanism underlying liver injury. ROS can trigger membrane lipid peroxidation, resulting in changes in membrane fluidity and permeability and the generation of lipid peroxides (LPOs), the main representative of which is malondialdehyde (MDA). MDA disrupts the integrity of the hepatocyte membrane and mitochondrial membrane, inhibits the function of membrane proteins, and causes liver tissue damage. Moreover, elevated MDA levels have been reported in the serum of patients with sepsis, whereas catalase (CAT) and superoxide dismutase (SOD) activities as well as serum glutathione (GSH) levels are reduced. Furthermore, MDA levels and SOD activity are correlated with the severity and prognosis of sepsis.

Nuclear factor-erythroid 2-related factor 2 (Nrf2) serves as a critical transcriptional regulator of cellular redox homeostasis [11]. In the context of inflammatory pathologies, including alcoholic liver disease and SALI, Nrf2 pathway activation potentiates endogenous antioxidant capacity while attenuating inflammatory cascades and subsequent tissue injury. The Kelch-like ECH-associated protein 1 (Keap1)/Nrf2 axis constitutes a redox-responsive signaling cascade that critically regulates cellular antioxidant responses [12]. Under physiological conditions, it critically maintains systemic redox balance and confers cellular protection against oxidative stress and exogenous insults. Pathologic oxidative stress is correlated with dysregulated NF-κB pathway activation. Elevated levels of endogenous ROS induce significant oxidative injury while concurrently activating the redox-sensitive transcription factor NF-κB, a pivotal mediator of proinflammatory signaling pathways [13]. Excessive pro-inflammatory cytokine production induces ROS generation, leading to oxidative damage and the development of a self-perpetuating pathological cycle. In addition, the protective effects of antioxidants have been demonstrated in animal models of sepsis. Collectively, these findings demonstrate that targeting redox imbalance represents a mechanistically grounded strategy for SALI management.

Angelicin (ANG), a natural furanocoumarin compound extracted from the dried ripe fruit of the legume *Psoralea corylifolia* Linn., possesses a variety of biological activities. The anti-inflammatory and antioxidative effects of ANG have attracted attention in recent years. Previous studies have demonstrated that, as an analogue of ANG, psoralen has potent anti-inflammatory effects through the downregulation of LPS-induced Toll-like receptor 4 (TLR4) expression and the phosphorylation of interleukin 1 receptor-associated kinase 4 (IRAK4) and p65, consequently suppressing NF-κB signal transduction. In addition, ANG reduces the phosphorylation levels of epidermal growth factor receptor (EGFR), protein kinase B (AKT) and IκB and inactivates the EGFR-mediated AKT signaling pathway, which in turn exerts anti-inflammatory effects. In preclinical models of inflammatory disorders, including periodontitis and osteoarthritis, ANG has exhibited significant anti-inflammatory efficacy. ANG has been reported to upregulate KAT6A expression, which activates the Nrf2/HO-1 antioxidant pathway, reduces intracellular ROS levels, and ultimately ameliorates oxidative stress in ovariectomized osteoporotic rats. In addition, ANG has been reported to increase the activities of endogenous antioxidant enzymes, such as SOD, glutathione peroxidase (GSH-Px) and CAT, thereby protecting cells from oxidative damage. However, the mechanism of the anti-inflammatory and antioxidant effects of ANG during SALI has not been fully elucidated.

In the present study, an *in vivo* SALI mouse model and an *in vitro* AML12 cell model were established through CLP surgery and LPS stimulation to investigate the therapeutic effects of ANG in the treatment of SALI and to further explore the underlying mechanisms involved.

Materials and Methods

Ethics statement

All animal handling and procedures were in accordance with the Chinese Guidelines for Ethical Review of Laboratory Animals-Animal Welfare and the National Research Council Guidelines for the Care and Use of Laboratory Animals. All animal experimental procedures were approved by the Animal Ethics Committee of Jiangsu Ocean University (No. 20240208005).

Chemicals and reagents

ANG (CAS: 523-50-2) was obtained from Solarbio (Beijing, China). Lipopolysaccharide (LPS, *Escherichia coli* 0111: B4) was obtained from Sigma-Aldrich (St Louis, USA). Protease, phosphatase inhibitor and universal tissue fixative were obtained from Biosharp (Hefei, China). Trizol reagent was obtained from Vazyme (Nanjing, China). 4′,6-Diamidino-2-phenylindole (DAPI) and dihydroethidium (DHE) probes were obtained from Beyotime (Beijing, China). Total antioxidant capacity (T-AOC), MDA, GSH and CAT assay kits

were obtained from Nanjing Jiancheng Bioengineering Institute (Nanjing, China). MonScript RTIII Super Mix and SYBR Green fluorescent quantitative PCR premix were obtained from Monad (Wuhan, China).

The following antibodies were used in this study: anti-IKKβ (8943S) and anti-p-IKKβ (2078T) were obtained from Cell Signaling (Danvers, USA). Anti-p65 (T55034S), anti-Bax (A12009) and anti-Bcl-2 (A0208) were obtained from ABclonal (Wuhan, China). Anti-IL-6 (WL02841), anti-IL-10 (WL03088), anti-IκBα (WL03419), anti-Nrf2 (WL02135) and anti-Keap1 (WL03285) were obtained from Wanleibio (Shenyang, China). Anti-p-p38 (IPH0015) and anti-p38 (IMB1155) were obtained from Baijia (Xuzhou, China). Anti-CYP2E1 (19937-1-AP), anti-p-p65 (82335-1-RR), anti-GAPDH (60004-1-Ig) and anti-mouse and anti-rabbit horseradish peroxidase-conjugated detection antibodies were obtained from Proteintech (Wuhan, China).

Animal experiments

Wild-type (WT) BALB/c male mice (6–8 weeks old, 20–22 g) were obtained from the Experimental Animal Center of Yangzhou University (Yangzhou, China), and the mice were acclimated for 7 days under controlled environmental conditions: 12/12-h light/dark photoperiod, ambient temperature maintained at 23 ± 2°C, and relative humidity regulated at 50% ± 10%. A total of 84 mice were equally divided into 7 groups with 12 mice in each group: (1) the sham operation group (Sham), (2) the sham operation group (Sham + 10 mg/kg ANG), (3) the sepsis group (CLP), (4) the low-dose ANG group (CLP + 2.5 mg/kg ANG), (5) the medium-dose ANG group (CLP + 5 mg/kg ANG), (6) the high-dose ANG group (CLP + 10 mg/kg ANG) and (7) the positive control drug dexamethasone (DEX) treatment group (CLP + 2.5 mg/kg DEX). The drug dosage was determined according to a previous study [14]. Each group was injected with the same volume of reagents after CLP surgery: saline was injected intraperitoneally in the Sham and CLP groups, the other groups were injected with their counterparts, and all the mice were placed on surgical thermostatic blankets after surgery until awakening. All reagent injections were administered 0 h after the Sham/CLP surgery and continued for 7 days. The mice were euthanized at the end of the experiment, and blood and liver tissue samples were collected for further study. Euthanasia is required when mice are unable to consume water and food on their own or when they lose more than 20% of their normal body weight.

A modified murine sepsis score (MSS) system was used to assess the mice following CLP procedures. The scoring system evaluated seven clinical parameters: general appearance, consciousness level, spontaneous activity, response to stimuli, eye condition, respiratory rate, and respiratory quality. Each parameter was scored on a 0–4 scale, with higher scores representing more severe disease manifestations. Only mice with MSS scores between 4 and 7 were included for subsequent drug administration and CLP model experiments. Euthanasia criteria were defined as either a total MSS score surpassing 21 points or a deterioration of > 3 points in respiratory parameters (rate or quality).

Cell culture

The mouse liver parenchymal cell line AML12 was obtained from the Institute of Basic Medical Sciences, Chinese Academy of Medical Sciences (Beijing, China), for *in vitro* studies. AML12 cells were cultured in high-sugar DMEM supplemented with 10% fetal bovine serum, 1% penicillin and streptomycin. AML12 cells were cultured in a sterile incubator at 37°C with 5% CO_2. All reagents and procedures were strictly aseptic, and all operations were performed in a biosafety chamber. Before LPS stimulation, the AML12 cells were pretreated with ANG (10/20 μM) for 2 h. Then, the AML12 cells were stimulated with 1 μg/mL LPS according to previous methods, and the cells were collected 24 h later for subsequent experiments. The dosage of LPS used was the same as previously described [15].

AML12 cells were inoculated into 96-well plates at a density of 1×10^5 cells/well and treated with different concentrations of ANG (0, 1, 2, 5, 10, 20, 50, 100, 200, or 500 μM) for 24 h. The CCK-8 reagent (Biosharp) was subsequently added, followed by incubation at 37°C for 2 h. The absorbance at 450 nm (OD_{450}) was measured. The safe administration concentration of ANG for AML12 was selected on the basis of the results.

Cell transfection

The p65 overexpression plasmid [pCMV-Rela(mouse)-3×FLAG-Neo; MiaoLingBio, Wuhan, China] was transfected using ExFect transfection reagent (Vazyme) for 24 h, after which the cells were exposed to LPS and ANG. After 48 h, the protein expression of p65 was detected by western blot analysis to verify the transfection efficiency.

Hematoxylin and eosin (H&E) staining

Liver tissues were removed quickly after the mice were euthanized, rinsed with saline, cut into small 1-cm^3 pieces on ice and fixed in universal tissue fixative overnight. The tissue blocks were then prepared into paraffin sections of liver tissue, which were sequentially deparaffinized and hydrated, followed by hematoxylin and eosin (H&E) staining, dehydration, permeabilization, and sealing. Histopathological examination was performed using a light microscope (DS-F12; Nikon, Tokyo, Japan), with representative images captured to document characteristic pathological alterations.

To evaluate the degree of liver tissue damage in the mice, sections of H&E-stained liver tissue were scored blindly by two pathologists on a 4-point scale. Briefly, 3 randomly selected high-magnification fields of view per slide were analyzed. The severity of liver injury was scored as follows: 0, minimal or no signs of injury; 1, mild injury, including cytoplasmic vacuolization and focal apoptosis; 2, moderate injury with extensive apoptosis, increased cytoplasmic eosinophilia, and loss of intercellular junctions; and 3, severe necrosis with hepatic cord disintegration, hemorrhage, and neutrophil infiltration.

Biochemical assay

Tissue samples of appropriate weight were processed by low-temperature homogenization in normal saline using a high-throughput homogenizer, with the tissue-to-saline volume ratios maintained at either 1:9 or 1:4 (v/v%). After adequate homogenization and low-speed centrifugation to remove the tissue precipitate, the homogenized supernatant was collected. In accordance with the method of tissue homogenization described in the instruction manual, the absorbance values reflecting T-AOC, MDA levels, GSH content, and CAT activity were measured spectrophotometrically at their respective optimal wavelengths (593 nm, 532 nm, 420 nm, and 405 nm) via a full-wavelength microplate reader. The tissue

redox parameters (content/activity) were normalized according to their respective standard calculation formulas.

Real-time fluorescence quantitative PCR (qPCR) analysis

For tissue or cell samples, 20 mg of liver tissue was accurately weighed, or AML12 cells in six-well plates were collected by digestion with cold PBS. Then, 1 mL of Trizol was added, and the mixture was placed in a high-throughput tissue grinder and fully homogenized before 200 μL of chloroform was added and fully mixed. The supernatant was then centrifuged at 12000 *g*, 500 μL of isopropanol was added to the supernatant, which was mixed thoroughly. The mixture was then incubated at 4°C for 10 min and centrifuged, and the supernatant was discarded. The white precipitate was then washed repeatedly with 75% ethanol. Following the final centrifugation step, the supernatant was carefully removed, and the resulting white precipitate was allowed to air dry at ambient temperature. Finally, the RNA was dissolved in DEPC water.

One microgram of RNA was reverse transcribed into cDNA using MonScript RTIII Super Mix. A 100-fold dilution of cDNA was used as a template for quantitative PCR (qPCR) with SYBR Green qPCR mix, and the expression levels of the genes were calculated relative to that of the housekeeping gene, *β-actin*, via the $2^{-\Delta\Delta CT}$ method. All primers were synthesized by Bioengineering (Shanghai, China), and the primer sequences are shown in Table 1.

Western blot (WB) analysis

For tissue or cell samples, 20 mg of liver tissue was accurately weighed, or AML12 cells in 6-well plates were collected via digestion with cold PBS, added to 100 μL of RIPA lysis buffer containing protease and phosphatase inhibitors, placed in a high-throughput tissue grinder, and centrifuged to remove the supernatant after sufficient homogenization. After the protein concentration was determined, 30 μg of proteins were separated by 12% SDS-PAGE, and transferred onto a PVDF membrane. The PVDF membrane containing the target protein was blocked in 5% non-fat milk for 2 h and then incubated with the corresponding primary antibody at 4°C for 12 h. Following this step, the samples were incubated with species-matched secondary antibodies at room temperature for 1 h. The final protein bands were visualized using enhanced chemiluminescence (ECL) reagent (Vazyme) and imaged with a multifunctional ultrasensitive imaging system, followed by quantitative protein analysis using ImageJ software. GAPDH was used as a loading control to determine the relative expression level of each protein.

DHE staining

Fresh mouse liver tissue was cut into small 1-cm^3 pieces on ice, and after fixation in universal tissue fixative, the blocks were prepared as frozen sections of liver tissue. The sections were then treated with 2 μM DHE for 30 min at 37°C, rinsed three times with PBS, and then restained with 2 μg/mL DAPI for 5 min. Images were acquired using a confocal microscope (Eclipse Ti2; Nikon).

Terminal deoxynucleotidyl transferase dUTP nick end labeling (TUNEL) staining

Fresh mouse liver tissue was cut into small 1-cm^3 pieces on ice and fixed in 4% paraformaldehyde, followed by dehydration, embedding, sectioning, and deparaffinization. The tissue sections were digested with proteinase K and washed with PBS, then subjected to apoptosis detection using a TUNEL detection kit (Vazyme), with cell nuclei counterstained by DAPI. Fluorescence signals on the stained sections were finally observed under a confocal microscope (Eclipse Ti2). Cells exhibiting bright red staining were identified as TUNEL-positive.

Flow cytometry for apoptosis detection

To assess apoptosis, an Annexin V-FITC/PI Apoptosis Detection Kit (G1511; Servicebio, Shanghai, China) was employed. Following the manufacturer's protocol, harvested cells were washed with PBS and resuspended in buffer solution. Subsequently, 1 μL Annexin V-FITC and 2 μL propidium iodide (PI) were sequentially added, followed by thorough mixing and incubation at room temperature in the dark for 10–15 min. Apoptotic cell populations were distinguished using a FACS Canto II flow cytometer (BD Biosciences, Franklin Lakes, USA), with double-negative cells serving as the viable reference population. Fluorescence intensity was analyzed using FlowJo (v10.8).

Statistical analysis

All experimental data were obtained from no less than three independent replications. Bar graphs were generated with GraphPad Prism 9.5 software, and the data were normally distributed. All the data are presented as the mean ± SEM. Independent samples *t* tests were used to compare two independent sample groups, one-way ANOVA was used to compare three or more sample groups, and Tukey's post hoc test was used to compare variables between groups. $P < 0.05$ was considered statistically significant.

Results

ANG protects against liver tissue damage in SALI mice

To evaluate the potential hepatoprotective effects of ANG against SALI in mice, hepatic histopathological alterations were assessed by H&E staining. Histopathological analysis revealed that the liver tissue of the mice in the CLP group exhibited extensive vacuolar degeneration of hepatocytes, many necrotic cells, and a disorganized cellular structure compared with that of the mice in the Sham group. In contrast, the liver tissues of the mice treated with ANG presented slight vacuolar degeneration of hepatocytes, which were neatly arranged, and the liver structure was relatively normal

Table 1. Sequences of primers used in this study

Gene	Forward primer (5′→3′)	Reverse primer (5′→3′)
Il-1β	TGCCTTCTTGGGACTGATGC	GCAAGTGCATCATCGTTGTTC
Il-6	AGGAGAACCAAGCAACGACA	CTCTGCTTGTGAGGTGCTGA
Tnf-α	GACGTGGAACTGGCAGAAGA	GGCTACAGGCTTGTCACTCG
Il-10	GCAGTGGAGCAGGTGAAGAG	CGGAGAGAGGTACAAACGAGG
β-actin	GCCATGTACGTAGCCATCCA	ACGCACGATTTCCCTCTCAG

(Figure 1A). These findings suggest that ANG has a protective effect against liver tissue injury in SALI mice. In addition, the histological scores similarly revealed that ANG intervention was able to reduce liver tissue injury after CLP (Figure 1B). To further investigate whether ANG could improve the dysfunction of liver tissues in SALI mice, the serum levels of ALT and AST were examined (Figure 1C, D). The results revealed that the serum levels of ALT and AST were significantly increased after CLP treatment compared with those in the Sham group, while ANG intervention was able to restore the levels of ALT and AST, indicating that ANG was able to alleviate liver tissue dysfunction in SALI mice.

ANG alleviates the inflammatory response to SALI in mice and LPS-stimulated AML12 cells

The liver has been reported to be a key organ for cytokine production and systemic inflammatory regulation during sepsis. Among hepatic parenchymal cells, upregulated TNF-α and IL-6 initiate proinflammatory signaling cascades, potentially inducing acute phase response activation, hepatocyte damage, and systemic inflammatory reactions [16]. To investigate whether ANG could alleviate the CLP-induced inflammatory response in mouse liver tissues, the transcript levels of the pro-inflammatory factors *Il-1β*, *Il-6*, and *Tnf-α* and the anti-inflammatory factor *Il-10* were detected in the liver tissues of all groups of mice via qPCR (Figure 2A–D). qPCR analysis revealed that the transcript levels of pro-inflammatory factors *Il-1β*, *Il-6*, and *Tnf-α* were significantly higher in the CLP group than in the Sham group, whereas the transcript level of the anti-inflammatory factor *Il-10* was significantly lower. Compared with the CLP group, the ANG-treated groups presented significantly lower transcript levels of the pro-inflammatory factors *Il-1β*, *Il-6*, and *Tnf-α* and restored transcript levels of the anti-inflammatory factor *Il-10*. These results suggest that ANG intervention can alleviate the inflammatory response of liver tissue in SALI mice. For further validation, the safe concentration of ANG for AML12 cells was initially determined by CCK-8 assay (Figure 2E). Similarly, the transcript levels of the pro-inflammatory factors *Il-1β*, *Il-6*, and *Tnf-α* and the anti-inflammatory factor *Il-10* were assayed in an *in vitro* model of LPS-stimulated AML12 (Figure 2F,I). The results revealed

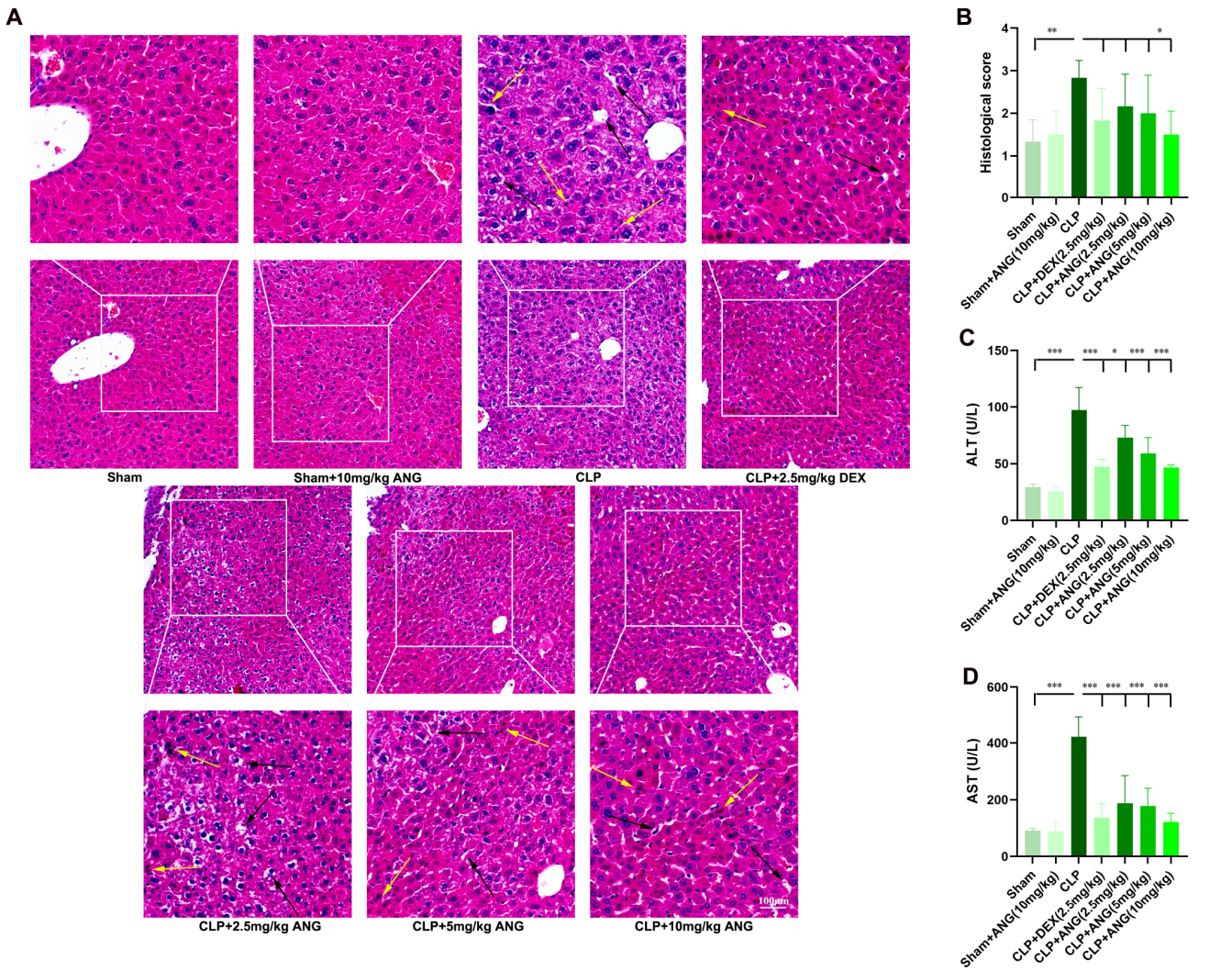


Figure 1. ANG alleviates liver tissue injury and dysfunction in SALI mice (A) Histopathological changes in the livers of the mice in each group were observed via H&E staining. The black arrows indicate vacuolar necrosis, and the yellow arrows indicate inflammatory infiltration. Scale bar: 100 μm. (B) Quantitative analysis of histopathological liver injury scores ($n = 6$). (C,D) Serum levels of ALT and AST in each group of mice ($n = 6$). Data are expressed as the mean ± SEM. $^{*}P < 0.05$, $^{**}P < 0.01$, $^{***}P < 0.001$.

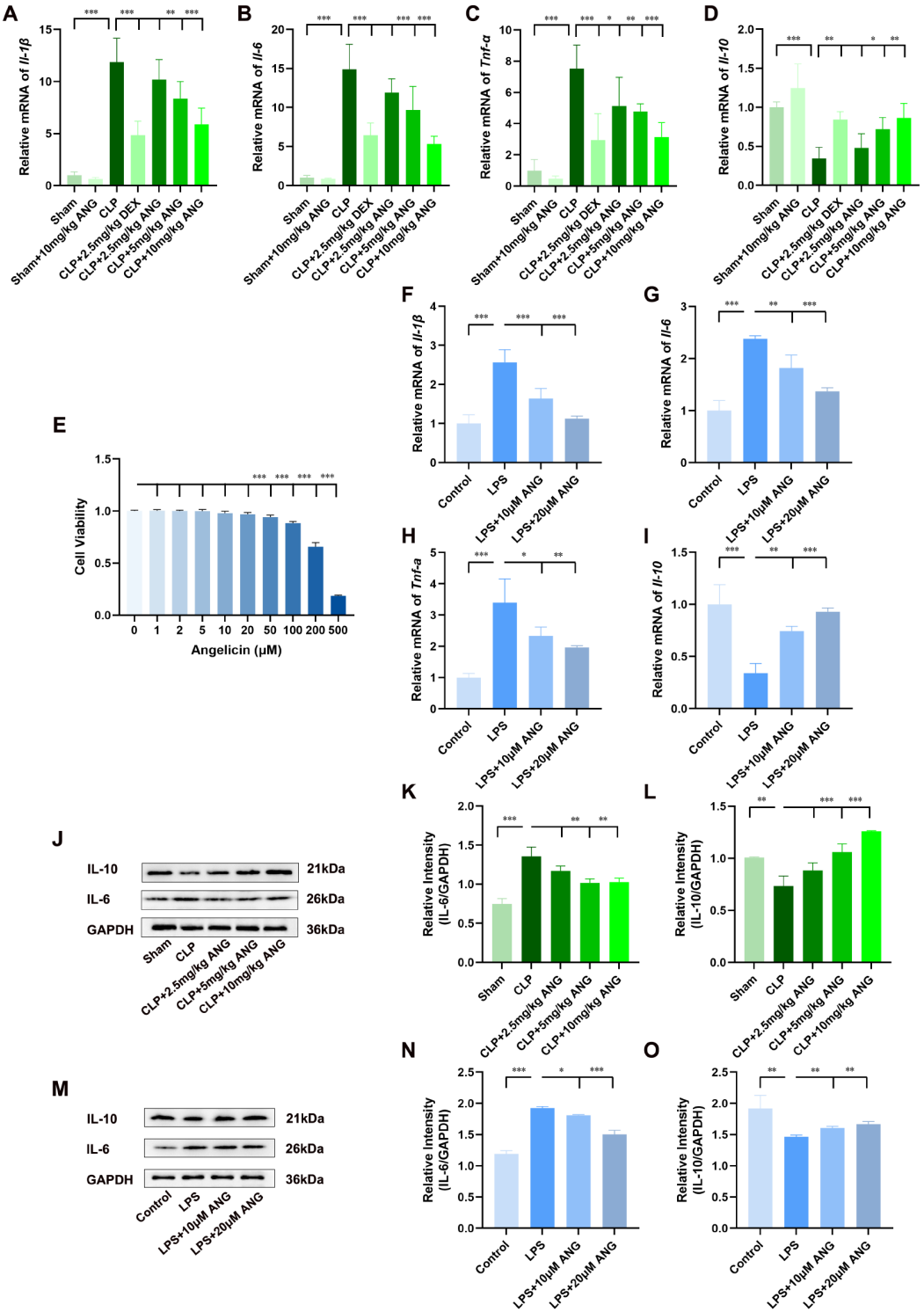


Figure 2. ANG alleviates the inflammatory response in liver tissue in SALI mice and in LPS-stimulated AML12 cells (A–D) The transcript levels of pro-inflammatory factors *Il-1β*, *Il-6*, and *Tnf-α* and the anti-inflammatory factor *Il-10* in the liver tissues of the mice in each group were detected by qPCR ($n = 6$). (E) Screening for safe concentrations of ANG in AML12 cells by CCK8 assay ($n = 3$). (F–I) Transcript levels of pro-inflammatory factors *Il-1β*, *Il-6*, and *Tnf-α* and the anti-inflammatory factor *Il-10* in each group of AML12 cells were detected by qPCR ($n = 6$). (J) Protein expression levels of IL-10 and IL-6 in the liver tissues of the mice in each group were detected by WB analysis. (K,L) Gray-scale analysis of the IL-10/GAPDH and IL-6/GAPDH ratios via ImageJ ($n = 3$). (M) Protein expression levels of IL-10 and IL-6 were detected by WB analysis in AML12 cells from each group. (N,O). Gray-scale analysis of IL-10/GAPDH and IL-6/GAPDH ratios via ImageJ ($n = 3$). Data are expressed as the mean ± SEM. $^{*}P < 0.05$, $^{**}P < 0.01$, $^{***}P < 0.001$.

that the transcript levels of pro-inflammatory factors *Il-1β*, *Il-6*, and *Tnf-α* were significantly reduced and that the transcript level of the anti-inflammatory factor *Il-10* was significantly increased after ANG treatment compared with those in the LPS group, suggesting that ANG was also able to inhibit inflammatory responses in an *in vitro* model of LPS-stimulated AML12.

In addition, the protein expression levels of the pro-inflammatory cytokine IL-6 and the anti-inflammatory cytokine IL-10 in the liver tissues of the mice were determined by WB analysis (Figure 2J–L). Compared with those in the Sham group, the mice in the CLP group presented significantly upregulated IL-6 expression, accompanied by downregulated IL-10 expression. However, following ANG treatment, the protein expression levels of IL-6 in the treatment groups were significantly lower than those in the CLP group, and the protein expression level of IL-10 was restored. Similarly, the protein expression levels of IL-6 and IL-10 in AML12 cells from each group were further examined by WB analysis (Figure 2M–O). Consistent with the *in vivo* findings, compared with control AML12 cells, AML12 cells in the LPS group presented significantly upregulated IL-6 expression, whereas IL-10 expression was significantly downregulated. Notably, ANG treatment significantly suppressed IL-6 expression and restored IL-10 expression. These findings indicate that ANG intervention can alleviate hepatic inflammatory responses in SALI.

ANG alleviates oxidative stress in SALI mice and LPS-stimulated AML12 cells

Oxidative stress has been reported to be an important mechanism in SALI. Under septic conditions, hepatic ROS generation is significantly augmented, which is driven primarily by excessive proinflammatory cytokine production and compromised mitochondrial function [17,18]. To investigate whether ANG can ameliorate oxidative stress in the liver tissues of SALI mice, relevant indices of antioxidant enzymes and peroxides, including T-AOC, MDA, GSH, and CAT, were detected using biochemical kits (Figure 3A–D). Compared with Sham treatment, CLP treatment significantly decreased T-AOC, GSH and CAT levels and significantly increased MDA levels. These findings suggest that oxidative stress occurs in the liver tissue of SALI mice. However, compared with the CLP group, ANG treatment significantly increased the levels of T-AOC, GSH and CAT and significantly decreased the level of MDA, suggesting that ANG was able to ameliorate oxidative stress in the liver tissue of SALI mice.

Cytochrome P450 2E1 (CYP2E1), a phase I metabolizing enzyme, is able to participate in the onset and progression of inflammatory diseases. CYP2E1 has been reported to disrupt mitochondrial function by increasing the production of ROS, thereby triggering oxidative stress and inflammation. To investigate whether ANG affects the protein expression of CYP2E1, the protein expression level of CYP2E1 in the liver tissues of each group of mice was detected by WB analysis (Figure 3E,F). The protein expression level of CYP2E1 was significantly increased after CLP treatment, whereas ANG treatment significantly inhibited the protein expression level of CYP2E1, suggesting that ANG may inhibit oxidative stress by suppressing the protein expression level of CYP2E1.

Oxidative stress is usually caused by a large accumulation of ROS in the body. To further validate the antioxidative stress effect of ANG, the ROS levels in the liver tissues of the mice in each group were detected by DHE staining (Figure 3G,H). Compared with Sham treatment, CLP treatment significantly increased the levels of ROS. ANG treatment significantly inhibited the levels of ROS, suggesting that ANG significantly inhibited the CLP-induced increase in the levels of ROS. In addition, the ROS levels of AML12 cells in each group were examined by flow cytometry (Figure 3I), and compared with those in the control group, the ROS levels in the LPS-treated group were significantly elevated. In contrast, ANG treatment significantly inhibited the levels of ROS, suggesting that ANG significantly inhibited the LPS-induced increase in the levels of ROS.

ANG inhibits activation of the NF-κB pathway

The NF-κB pathway is not only a key regulator of the inflammatory response but also capable of influencing oxidative stress by modulating the expressions of antioxidant enzymes (superoxide dismutase, catalase, *etc.*) [19]. To investigate whether ANG intervention could regulate the activation of the NF-κB pathway, the key proteins in the NF-κB pathway, p-IKKβ, IKKβ, IκBα, p-p65, and p65, were detected by WB analysis (Figure 4A–D). Compared with those in the Sham group, the protein expression levels of p-IKKβ and p-p65 were significantly increased, and the protein expression level of IκBα was significantly decreased in the liver tissues of mice after CLP treatment, suggesting that the NF-κB pathway was activated after CLP treatment. In contrast, the protein expression levels of p-IKKβ and p-p65 were significantly inhibited, and the protein expression level of IκBα was significantly increased after ANG treatment, suggesting that activation of the NF-κB pathway was significantly inhibited after ANG treatment. For further validation, the key proteins in the NF-κB pathway were similarly detected in an *in vitro* model of LPS-stimulated AML12 (Figure 4E–H). The results revealed that the protein expression levels of p-IKKβ and p-p65 were significantly inhibited and that the protein expression level of IκBα was significantly increased after ANG treatment compared with those in the LPS group, suggesting that ANG was also able to inhibit the activation of the NF-κB pathway in the LPS-stimulated *in vitro* model.

ANG inhibits activation of the p38 MAPK pathway

Activation of the MAPK pathway promotes cytokine production, which in turn promotes the body's inflammatory response and exacerbates multi-organ damage [20]. Increased p38 phosphorylation (p-p38) or p38 activity has been reported to exacerbate sepsis and posttraumatic inflammation [21,22]. To investigate whether ANG treatment could inhibit the activation of the p38 MAPK pathway, the key proteins of the p38 MAPK pathway, p-p38 and p38, were detected by WB analysis in the liver tissues of the mice (Figure 5A,B). The protein expression level of p-p38 was significantly higher in the CLP group than in the Sham group, suggesting that the p38 MAPK pathway was significantly activated in septic liver tissues. In contrast, the protein expression level of p-p38 was significantly lower in the ANG group than in the CLP group, suggesting that ANG treatment inhibited the CLP-induced activation of the p38 MAPK pathway. To further validate the inhibition of p38 MAPK pathway activation by ANG, the protein expression levels of p-p38 and p38 were also examined in an *in vitro* model of LPS-stimulated AML12 cells by WB analysis (Figure 5C,D). Compared with that in the control group, the protein expression of p-p38 was significantly elevated after LPS stimulation, whereas ANG treatment significantly inhibited the increase in p-p38 protein expression induced by LPS stimulation. These findings suggest that ANG

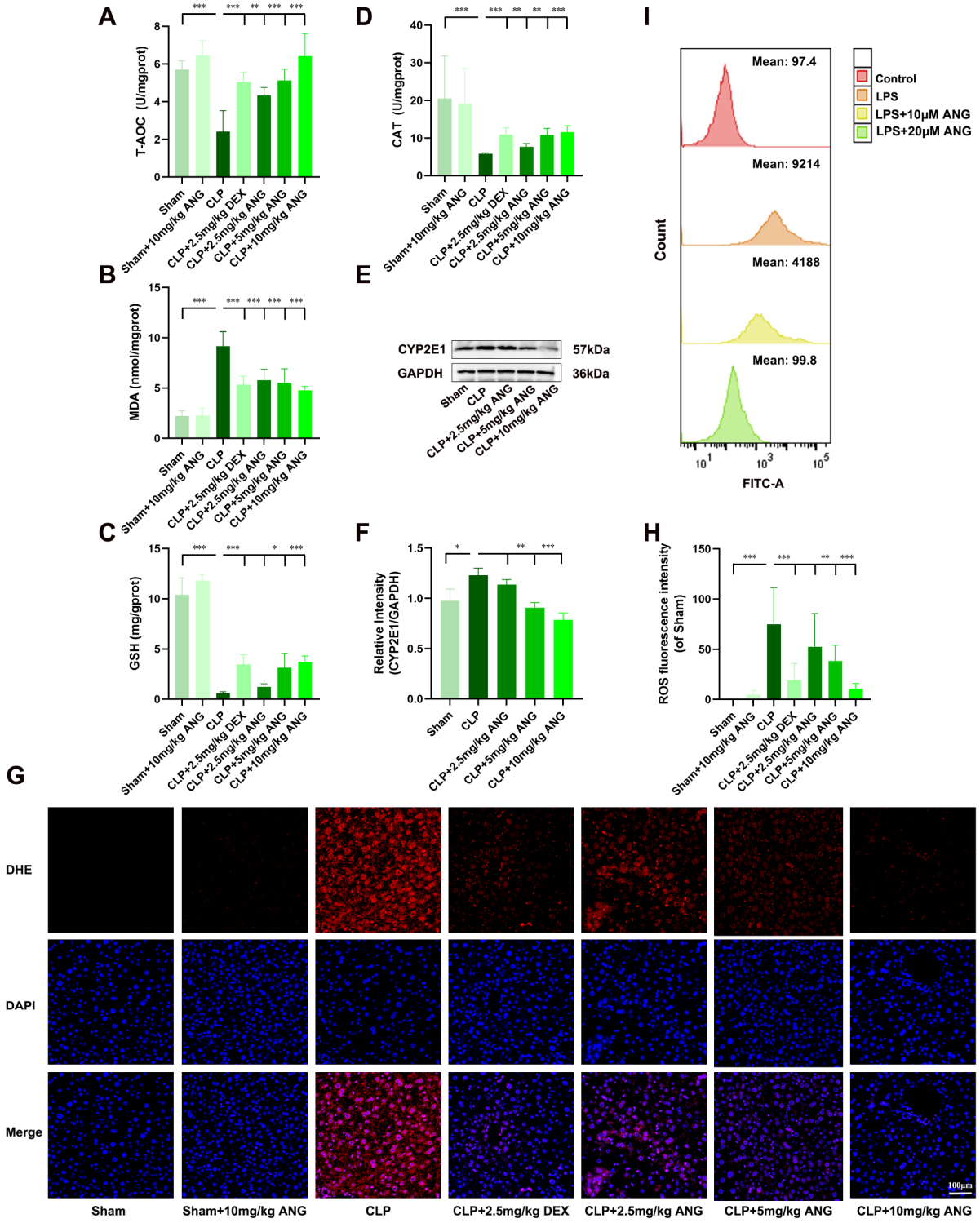


Figure 3. ANG alleviates oxidative stress in liver tissue in SALI mice and in LPS-stimulated AML12 cells (A–D) Liver tissue levels of T-AOC, MDA, GSH and CAT were detected via biochemical kits in all groups of mice ($n = 6$). (E) The protein expression levels of CYP2E1 in the liver tissues of each group of mice were detected by WB analysis. (F) Gray scale analysis of CYP2E1/GAPDH by ImageJ ($n = 3$). (G) The ROS levels in the liver tissues of the mice in each group were detected by DHE staining. Scale bar: 100 μm. (H) Results from the quantitative analysis of the ROS fluorescence intensity in the liver tissue sections of the mice in each group. (I) The ROS levels in the AML12 cells in each group were detected by flow cytometry. Data are expressed as the mean ± SEM. $^{*}P < 0.05$, $^{**}P < 0.01$, $^{***}P < 0.001$.

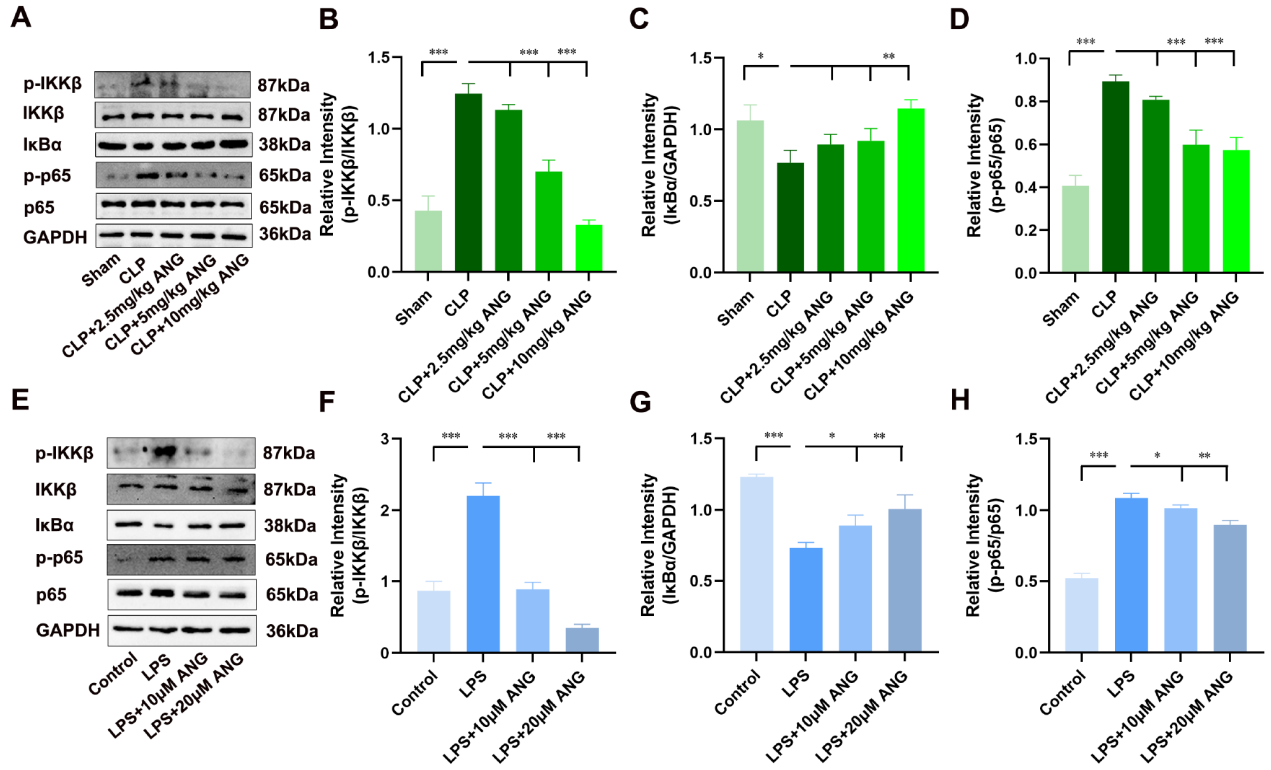


Figure 4. ANG inhibits the activation of the NF-κB pathway (A) The protein expression levels of p-IKKβ, IKKβ, IκBα, p-p65 and p65 in the liver tissues of the mice in each group were detected by WB analysis. (B–D) Gray-scale analysis of p-IKKβ/IKKβ, IκBα/GAPDH, and p-p65/p65 levels via ImageJ ($n = 3$). (E) Protein expression levels of p-IKKβ, IKKβ, IκBα, p-p65 and p65 were detected by WB analysis in AML12 cells from each group. (F–H). Gray-scale analysis of p-IKKβ/IKKβ, IκBα/GAPDH, and p-p65/p65 was performed via ImageJ ($n = 3$). Data are expressed as the mean ± SEM. $^{*}P < 0.05$, $^{**}P < 0.01$, $^{***}P < 0.001$.

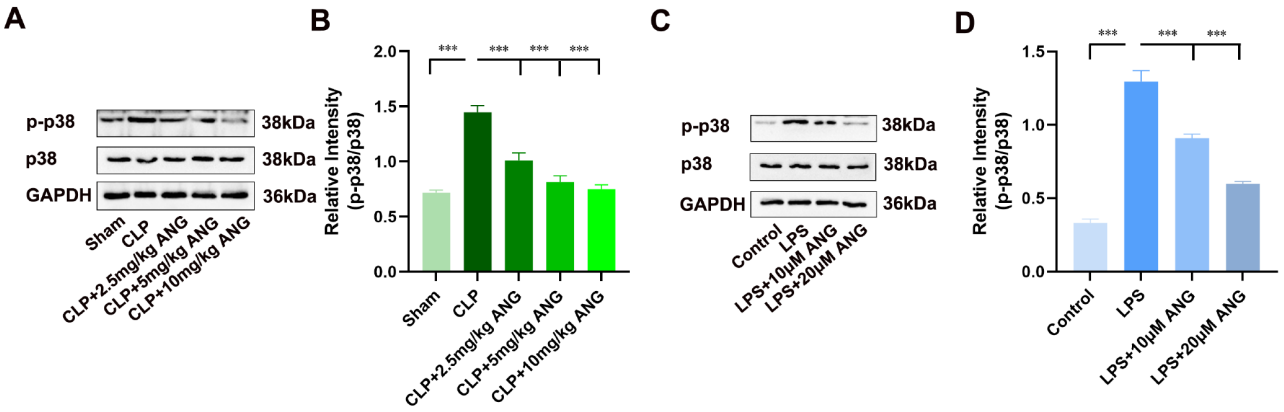


Figure 5. ANG inhibits the activation of the p38 MAPK pathway (A) Protein expression levels of p-p38 and p38 in the liver tissues of the mice in each group were detected by WB analysis. (B) Gray-scale analysis of p-p38/p38 levels via ImageJ ($n = 3$). (C) Protein expression levels of p-p38 and p38 were detected by WB analysis in AML12 cells from each group. (D) Gray-scale analysis of p-p38/p38 expression via ImageJ ($n = 3$). Data are expressed as the mean ± SEM. $^{***}P < 0.001$.

inhibits the activation of the p38 MAPK pathway.

ANG alleviates the inhibition of the Nrf2/Keap1 pathway

Nrf2 is an important transcription factor responsible for regulating the cellular response to oxidative stress [23]. The Nrf2/Keap1 pathway plays a crucial role in the antioxidant stress response and protection of hepatocytes from injury [24]. To investigate whether ANG treatment could alleviate the CLP-induced inhibition of the Nrf2/Keap1 pathway, the key proteins of the Nrf2/Keap1 pathway, Nrf2 and Keap1, were detected by WB analysis in the liver tissues of the mice (Figure 6A–C). Compared with that in the Sham group, the protein expression level of Nrf2 was significantly decreased, whereas that of Keap1 was significantly increased after CLP treatment. However, ANG treatment significantly increased the protein expression level of Nrf2 and decreased the protein expression level of Keap1 compared with those in the CLP group.

These findings suggest that the Nrf2/Keap1 pathway was significantly inhibited by CLP, whereas ANG alleviated the CLP-induced inhibition of the Nrf2/Keap1 pathway. For further validation, the protein expression levels of Nrf2 and Keap1 were examined via WB analysis in an *in vitro* model of AML12 cells (Figure 6D–F). Compared with that in the control group, the protein expression of Nrf2 was significantly lower and that of Keap1 was significantly greater after LPS stimulation, whereas ANG treatment significantly increased the protein expression of Nrf2 and significantly inhibited the protein expression of Keap1. These findings suggest that ANG can activate the Nrf2/Keap1 pathway.

ANG activates the Nrf2/Keap1 pathway through NF-κB inhibition to alleviate inflammation and oxidative stress

Different levels of activating molecules in the NF-κB signaling pathway (*e.g.*, the negative regulatory protein IκBα) are able to negatively regulate the Nrf2 pathway while activating NF-κB [25]. To elucidate the specific molecular targets through which ANG modulates inflammatory responses and oxidative stress, protein-protein interaction (PPI) network analysis was performed (Supplementary Figure S1). This analysis revealed functional interactions among key proteins, including Nos2, Chuk, Rela, Stat3, Hdac1, Sp1, Mapk1, Map3k11, and Hif1a, all of which are critically involved in inflammatory signaling pathways and oxidative stress regulation. Notably, PPI network revealed Rela (NF-κB p65) as a central node in these interactions. Subsequent molecular docking analysis between ANG and Rela yielded a binding score of –4.834 (Supplementary Figure S1B,C), suggesting that Rela is a potential direct target of ANG. To explore the specific mechanisms by which ANG regulates inflammation and oxidative stress, the pCMV-Rela (mouse)-3×FLAG-Neo plasmid, which overexpresses p65, was used for cell transfection in AML12 cells. After p65 was overexpressed, the protein expression level of p65 was first detected by WB analysis to verify the transfection efficiency (Figure 7A,B). The protein expression levels of Nrf2 and Keap1 in the Nrf2/Keap1 pathway were subsequently detected by WB analysis (Figure 7C–F). Compared with that in the LPS group, the protein expression level of Nrf2 was significantly higher, whereas that of Keap1 was significantly lower in the ANG-treated group. However, after LPS and ANG cotreatment, the protein expression level of Nrf2 was still

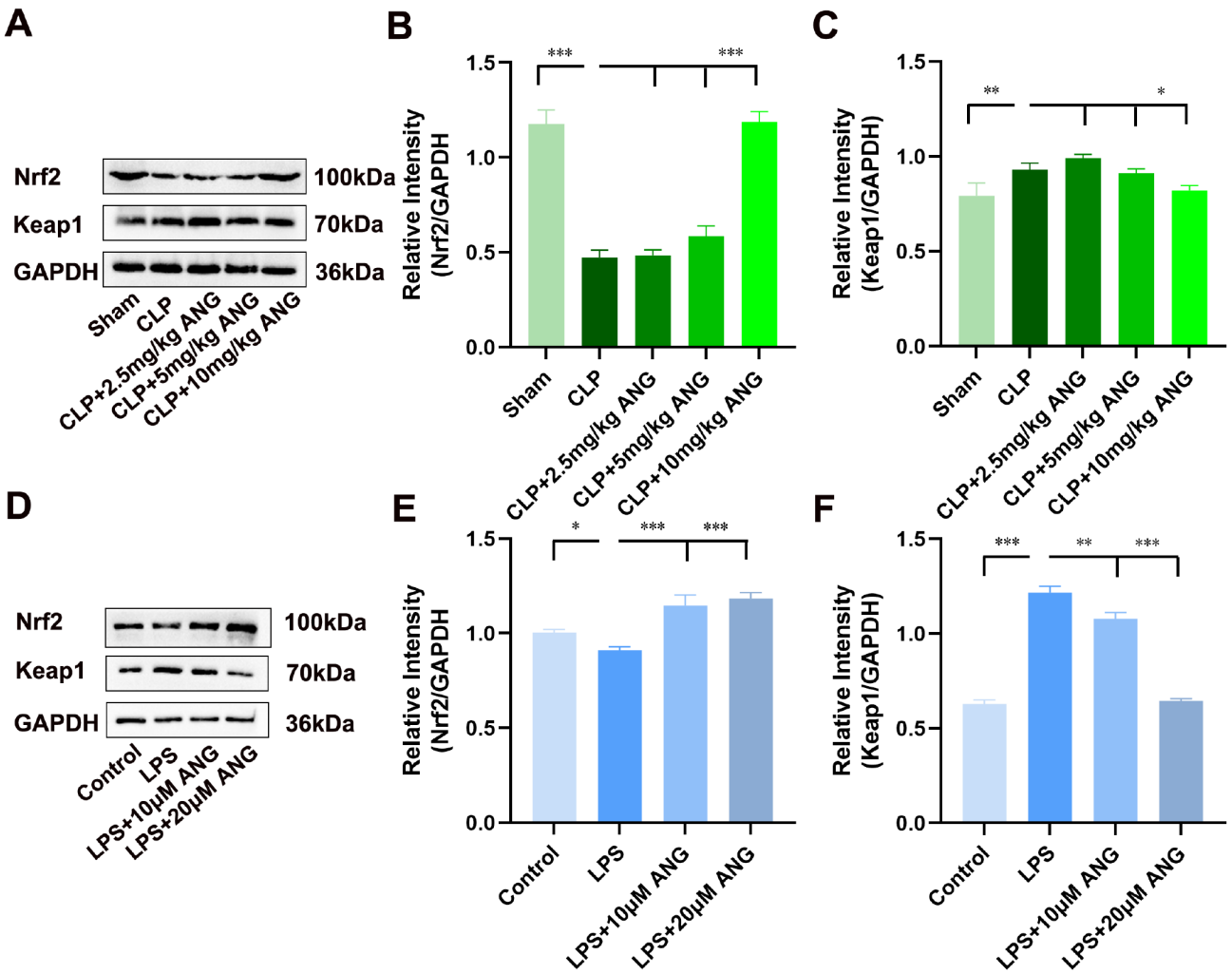


Figure 6. ANG can activate the Nrf2/Keap1 pathway (A) The protein expression levels of Nrf2 and Keap1 in the liver tissues of the mice in each group were detected by WB analysis. (B,C) Gray-scale analysis of Nrf2/GAPDH and Keap1/GAPDH levels via ImageJ (n = 3). (D) The protein expression levels of Nrf2 and Keap1 were detected by WB analysis in AML12 cells from each group. (E,F) Gray-scale analysis of Nrf2/GAPDH and Keap1/GAPDH levels via ImageJ (n = 3). Data are expressed as the mean ± SEM. *P < 0.05, **P < 0.01, ***P < 0.001.

significantly lower and that of Keap1 was significantly higher in the group transfected with the expression plasmid than in the group not transfected with the expression plasmid. These findings suggested that ANG treatment alleviated the LPS-induced inhibition of the Nrf2/Keap1 pathway, whereas overexpression of p65 reversed the alleviating effect of ANG. Collectively, these data suggest that ANG may exert its regulatory effects on the Nrf2/Keap1 pathway by attenuating NF-κB signaling, leading to increased Nrf2/Keap1 transcriptional activity.

We further validated whether ANG could regulate inflammation and oxidative stress by inhibiting the activation of the NF-κB pathway. The transcript levels of the pro-inflammatory factors *Il-1β*, *Il-6* and *Tnf-α*, and the anti-inflammatory factor *Il-10* were detected by qPCR (Figure 7G–J). After LPS and ANG co-treatment, the transcript levels of the pro-inflammatory factors *Il-1β*, *Il-6*, and *Tnf-α*, as well as the level of the anti-inflammatory factor *Il-10*, were still significantly elevated in the group transfected with the expression plasmid compared with those in the group not transfected with the expression plasmid, suggesting that overexpression of p65 reversed the anti-inflammatory effect of ANG. In addition, the ROS levels of AML12 cells in each group after p65 overexpression were detected by flow cytometry (Figure 7K), and after LPS and ANG co-treatment, the levels of ROS were significantly elevated in the group transfected with the expression plasmid compared with those in the group not transfected with the expression plasmid, suggesting that the overexpression of p65 reversed the antioxidative stress effect of ANG.

ANG alleviates apoptosis in SALI mice and LPS-stimulated AML12 cells

To investigate whether ANG could alleviate hepatic tissue apoptosis induced by CLP in mice, TUNEL staining was conducted on liver tissue sections from all groups (Figure 8A,B). Compared with that in the Sham group, the ratio of TUNEL-positive apoptotic cells in the CLP group was significantly higher. However, ANG treatment significantly reduced the level of apoptosis in mouse liver tissues. These results suggested that significant apoptosis occurred in mouse liver tissues following CLP, and ANG treatment alleviated CLP-induced apoptosis. To further explore the specific mechanism by which ANG mitigates apoptosis, the protein expression profiles of the apoptosis regulators Bcl-2 and Bax in the liver tissues of each group of mice were assessed by WB analysis (Figure 8C–E).

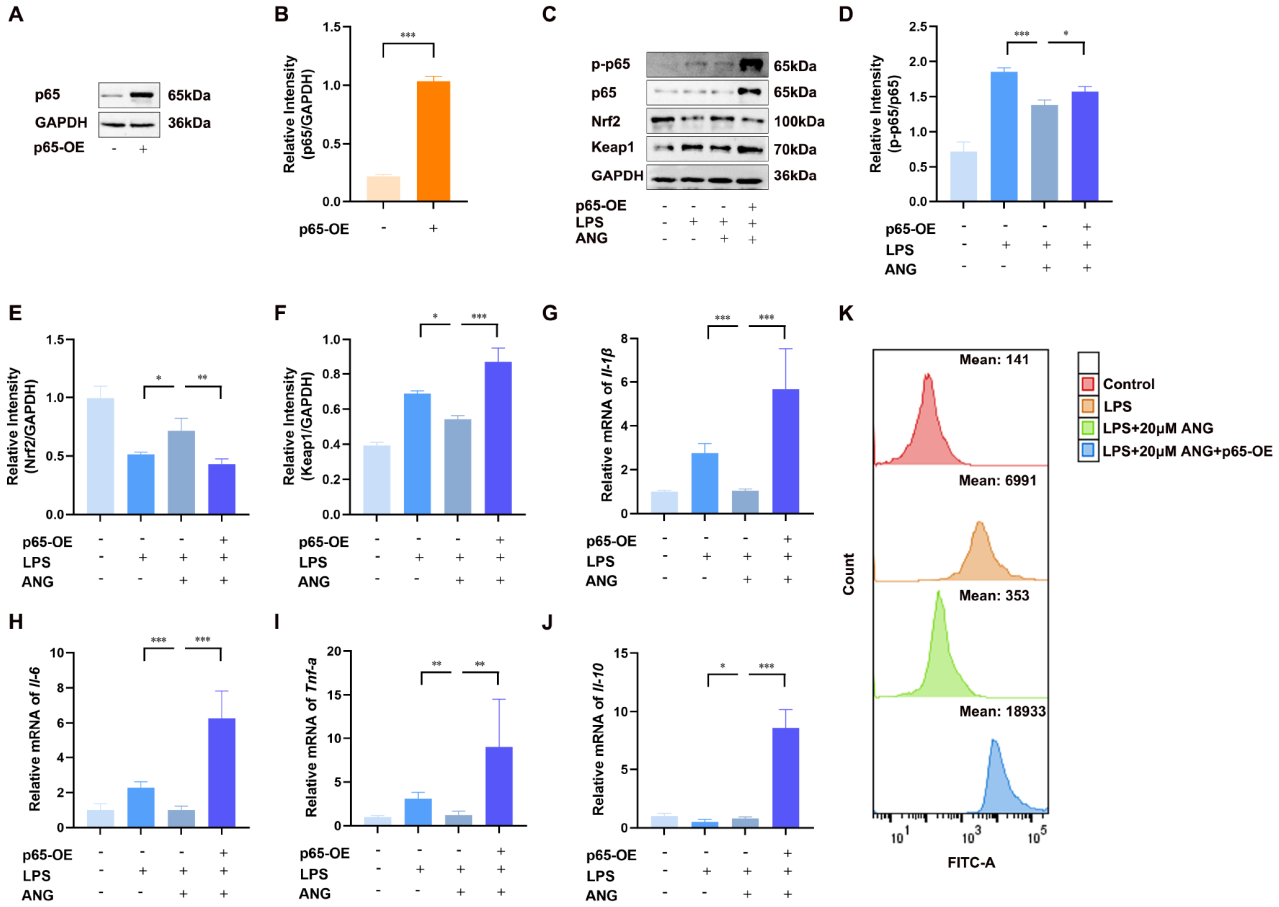


Figure 7. ANG alleviates LPS-stimulated inflammation and oxidative stress in AML12 cells by inhibiting the NF-κB pathway, which activates the Nrf2/Keap1 pathway (A) Protein expression levels of overexpressed p65 were detected by WB analysis. (B) Gray scale analysis of p65/GAPDH by ImageJ ($n = 3$). (C) Protein expression levels of p-p65, p65, Nrf2 and Keap1 in AML12 cells in each group after overexpression of p65 were detected by WB analysis. (D–F) Grayscale analysis of p-p65/p65, Nrf2/GAPDH, and Keap1/GAPDH by ImageJ ($n = 3$). (G–J) Transcript levels of pro-inflammatory factors *Il-1β*, *Il-6*, and *Tnf-α* and the anti-inflammatory factor *Il-10* in AML12 cells in each group after overexpression of p65 were detected by qPCR ($n = 6$). (K) The ROS levels in AML12 cells in each group after overexpression of p65 were detected by flow cytometry. Data are expressed as the mean ± SEM. $^*P < 0.05$, $^{**}P < 0.01$, $^{***}P < 0.001$.

Compared with that in the Sham group, Bax expression was significantly increased, whereas Bcl-2 expression was significantly decreased in the CLP group. In contrast, following ANG treatment, Bax expression was significantly reduced, whereas Bcl-2 expression was significantly increased compared with that in the CLP group. For further validation, the protein expression levels of Bcl-2 and Bax

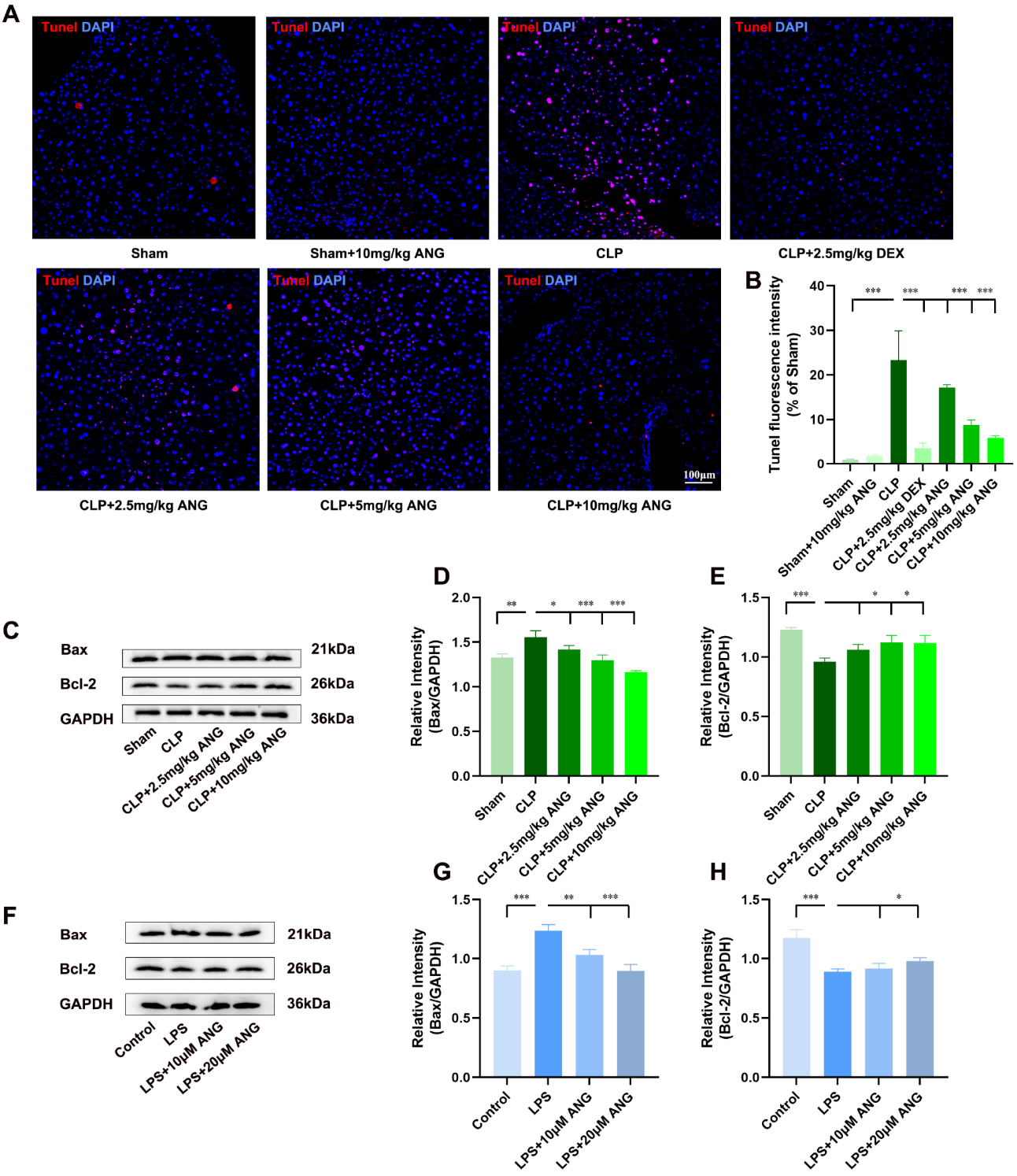


Figure 8. ANG alleviates apoptosis in liver tissue in SALI mice and LPS-stimulated AML12 cells (A) TUNEL staining was performed to observe hepatocyte death. Scale bar: 100 μm. (B) Quantitative analysis of TUNEL-positive fluorescence intensity in each group. (C) The protein expression levels of Bcl-2 and Bax in the liver tissues of each group of mice were detected by WB analysis. (D,E) Gray scale analysis of Bcl-2/GAPDH and Bax/GAPDH by ImageJ ($n = 3$). (F) The protein expression levels of Bcl-2 and Bax in AML12 cells in each group were detected by WB analysis. (G,H) Gray scale analysis of Bcl-2/GAPDH and Bax/GAPDH by ImageJ ($n = 3$). Data are expressed as the mean ± SEM. $^*P < 0.05$, $^{**}P < 0.01$, $^{***}P < 0.001$.

in LPS-stimulated AML12 cells were also assessed by WB analysis (Figure 8F–H). The results were consistent with those obtained from the *in vivo* experiments. Compared with that in the control group, Bax expression was significantly elevated, whereas Bcl-2 expression was significantly decreased in the LPS group. However, compared with that in the LPS group, Bax expression was significantly reduced, whereas Bcl-2 expression was significantly increased in AML12 cells following ANG treatment. These results demonstrated that ANG inhibited apoptosis by suppressing Bax protein expression and promoting Bcl-2 protein expression.

Discussion

Sepsis represents a life-threatening systemic inflammatory condition initiated by pathogenic infection, marked by profound immune homeostasis disruption that progresses to multiple organ dysfunction syndrome and potentially fatal organ failure [1]. The liver is one of the most vulnerable organs during sepsis, and abnormal liver function triggered by liver injury can exacerbate the sepsis process. The mitigation of SALI may be an important tool in the treatment of sepsis and in improving the survival of septic patients [26]. This study was conducted to elucidate the therapeutic potential of ANG against SALI and to delineate its underlying molecular mechanisms by establishing a SALI mouse model and an *in vitro* model using LPS-stimulated AML12 cells, with the potential to provide drugs for the treatment of SALI.

Psoralea corylifolia Linn. is a traditional Chinese medicine that can warm and tonify the kidney yang, replenish vital energy to alleviate respiratory distress, and use warm therapy to regulate splenic function to achieve antidiarrheal effects. Its pharmacological activity is attributed mainly to a variety of chemical constituents. In recent years, the anti-inflammatory effects of psoralens have received much attention. Psoralen has been reported to inhibit the inflammatory response in chondrocytes by activating estrogen receptors [27]. Psoralen can attenuate chemokines through the JAK2/STAT1 pathway and ameliorate CSE-induced airway inflammation in mice [28]. Similarly, ANG, one of the active components of psoralen, also has anti-inflammatory properties. ANG significantly attenuates the inflammatory response in mice with periodontitis [29]. In this study, ANG significantly inhibited the transcript levels of the pro-inflammatory factors *Il-1β*, *Il-6*, and *Tnf-α* and significantly increased the transcript level of the anti-inflammatory factor *Il-10* in the liver tissues of SALI mice, suggesting that ANG alleviated the inflammatory response in the liver tissues of SALI mice. In previous studies, intraperitoneal injection of LPS was used to establish an acute lung injury model that induced inflammation in the lungs of mice, whereas ANG pretreatment was able to reduce the production of the pro-inflammatory cytokines IL-6 and TNF-α [14], which is in full agreement with the findings of this study.

The inflammatory response can further exacerbate inflammatory injury by inducing the accumulation of immune cells such as neutrophils and macrophages in liver tissue, causing immune cell infiltration and the release of large amounts of ROS, which in turn contributes to oxidative stress [30]. T-AOC, MDA, GSH and CAT are key indicators for assessing oxidative stress and antioxidant status [31]. To investigate whether ANG can alleviate oxidative stress in the liver tissues of SALI mice, the levels of T-AOC, MDA, GSH and CAT were measured via biochemical kits. The results revealed that in the liver tissues of SALI mice, MDA levels were elevated, while the GSH content and CAT activity were reduced, and the T-AOC was decreased. These findings suggest that oxidative stress is exacerbated in the liver tissues of SALI mice. After ANG treatment, the MDA level decreased, whereas the GSH content and CAT activity increased, and the T-AOC also increased, suggesting that ANG alleviated oxidative stress in the liver tissues of SALI mice. In previous studies, GSH, GSH-PX, SOD and CAT levels in rat serum were significantly reduced in an OVX female rat model. In contrast, the levels of GSH, GSH-PX, SOD and CAT in rat serum increased in a dose-dependent manner after ANG treatment [32]. These findings suggest that ANG can alleviate oxidative stress in the OVX female rat model, which is in full agreement with the findings of this study.

The NF-κB signaling cascade represents a crucial intracellular transduction mechanism that orchestrates diverse pathophysiological processes, including inflammatory responses, immunoregulation, cellular viability, mitotic activity, and programmed cell death (apoptosis). It plays a key role in inflammatory diseases. In this study, the NF-κB pathway was overactivated in SALI mice, and ANG treatment significantly inhibited the protein expression level of p-p65, suggesting that ANG could alleviate the inflammatory response in the liver tissues of SALI mice through the inhibition of the NF-κB pathway, which is also consistent with previous studies. The MAPK pathway, which comprises the ERK, JNK, and p38 MAPK subfamilies, serves as a pivotal regulator by phosphorylating pro-inflammatory mediators that promote hepatic inflammation. This pathway is involved in oxidative stress and inflammatory responses, and its pathological overactivation induces cellular injury. The MAPK pathway was reported to be significantly activated during CLP-induced SALI, and the p38 MAPK pathway was shown to mediate cellular inflammation [33]. Therefore, in this study, the activation of the p38 MAPK pathway was the focus. CLP significantly increased the protein expression of p-p38, which suggested that the p38 MAPK pathway was significantly activated, whereas ANG treatment significantly suppressed p-p38 protein expression, suggesting that ANG treatment attenuated CLP-induced activation of the p38 MAPK pathway. In a previous study, ANG was shown to induce ATDC5 cell differentiation by modulating the p38 MAPK pathway [34]. In LPS-induced ALI, ANG blocked the phosphorylation of IκBα, NF-κB p65, and p38 MAPK [14], which is in full agreement with the findings of this study.

Nrf2 serves as a master regulator of cellular redox homeostasis, orchestrating the transcriptional upregulation of numerous antioxidant enzymes. This cytoprotective mechanism facilitates efficient neutralization of ROS, thereby mitigating oxidative stress-induced impairment of cellular architecture and physiological functions. Accumulating evidence has shown that Nrf2 activation has significant hepatoprotective effects. Our findings demonstrated that Nrf2 protein expression was significantly inhibited in the liver tissues of SALI mice and that this inhibition was ameliorated by ANG treatment. In addition, CLP treatment resulted in elevated Keap1 expression, which was also reversed by ANG treatment. These results suggest that ANG can alleviate liver oxidative stress by activating Nrf2-mediated antioxidant defense mechanisms. In a previous study, ANG was able to reduce oxidative stress by increasing the level of KAT6A in osteoblasts, further activating the Nrf2/HO-1 antioxidant system and decreasing the levels of ROS in osteoblasts [32], which is in full agreement with the findings of this study. Previous studies have identified CYP2E1 as a potential therapeutic target in sepsis because of its well-established role in mediating inflammatory processes and oxidative stress [35]. The

role of CYP2E1 in LPS-induced inflammation has been extensively documented [36,37]. For example, CYP2E1 has been demonstrated to transcriptionally regulate NLRP3 expression, while its inhibition effectively suppresses NF-κB activation [38]. Furthermore, studies have reported that abnormal elevation of hepatic CYP2E1 increases oxidative stress, subsequently leading to endoplasmic reticulum stress, mitochondrial dysfunction, and hepatocyte apoptosis [39]. The administration of CYP2E1 inducers significantly enhances LPS-induced oxidative stress in mouse liver tissues, and this effect is reversed by CYP2E1 inhibitors [40]. This effect may be associated with the Nrf2/Keap1 pathway, and further investigation is warranted to elucidate the exact molecular mechanisms involved, although this association was not thoroughly investigated in the present study.

To further explore the specific mechanisms by which ANG regulates inflammation and oxidative stress, a plasmid capable of overexpressing p65 was transfected into AML12 cells, which were then stimulated with LPS. ANG activated Nrf2 through NF-κB inhibition to alleviate inflammation and oxidative stress. Further analysis using qPCR and flow cytometry revealed that overexpression of p65 reversed the ameliorative effects of ANG on inflammation and oxidative stress. The crosstalk effect of the NF-κB pathway on the Nrf2 pathway has been similarly reported in other models, *e.g.*, chlorogenic acid reduces oxidative stress and neuroinflammation in the hippocampus of PTSD rats by modulating the crosstalk between the NF-κB and Nrf2 pathways [41]. This might be due to the ability of p65 to increase the nuclear accumulation of Keap1, which blocks Nrf2-ARE and reduces the production of cytoprotective enzymes [42].

Although the present study revealed a potential mechanism for the anti-inflammatory and antioxidative effects of ANG, there are differences in physiological and immune responses in humans because of the use of mice as an animal model of sepsis in this study. Although the present study explored the modulatory effects of ANG on the NF-κB, p38 MAPK, and Nrf2/Keap1 pathways, the pathway modulation and target effects were further validated *in vivo*. In the present study, ANG was administered for only seven consecutive days; therefore, this study focused on the short-term effects of ANG. In addition, despite the favorable therapeutic potential of ANG in this study, its clinical application still faces challenges related to dosage, route of administration, and drug stability.

In summary, an *in vivo* SALI model was established in mice via CLP, and an *in vitro* sepsis model was generated using LPS-stimulated AML12 cells. ANG attenuates SALI by suppressing the p38 MAPK pathway and activating the Nrf2/Keap1 pathway through the inhibition of NF-κB pathway. Overall, ANG mitigates hepatic inflammation and oxidative stress in SALI mice.

Supplementary Data

Supplementary data are available at *Acta Biochimica et Biophysica Sinica* online.

Funding

This work was supported by the grants from the Postgraduate Research & Practice Innovation Program of Jiangsu Ocean University (No. KYCX2024-18), the Lianyungang Traditional Chinese Medicine Science and Technology Development Plan Project (No. YB202203), the Science and Technology Funds of Kangda College, Nanjing Medical University (KD2024KYJJ085), the Jiangsu Society of Traditional Chinese Medicine Research Project (CYTF2024063), the Jiangsu Provincial Pharmaceutical Association-Aosaikang Hospital Pharmaceutical Research Fund Project (A202435) and the Priority Academic Program Development of Jiangsu Higher Education Institutions of China.

Conflict of Interest

The authors declare that they have no conflict of interest.

References

1. Singer M, Deutschman CS, Seymour CW, Shankar-Hari M, Annane D, Bauer M, Bellomo R, *et al.* The third international consensus definitions for sepsis and septic shock (Sepsis-3). *JAMA* 2016, 315: 801–810
2. Strnad P, Tacke F, Koch A, Trautwein C. Liver-guardian, modifier and target of sepsis. *Nat Rev Gastroenterol Hepatol* 2017, 14: 55–66
3. Mohyeldin RH, Alaaeldin R, Sharata EE, Attya ME, Elhamadany EY, Fathy M. LCZ696 attenuates sepsis-induced liver dysfunction in rats; the role of oxidative stress, apoptosis, and JNK1/2-P38 signaling pathways. *Life Sci* 2023, 334: 122210
4. Hotchkiss RS, Monneret G, Payen D. Sepsis-induced immunosuppression: from cellular dysfunctions to immunotherapy. *Nat Rev Immunol* 2013, 13: 862–874
5. Matsuda N, Machida T, Hattori Y. Molecular mechanisms underlying the pathogenesis of septic multiple organ failure. *Folia Pharmacol Jpn* 2024, 159: 101–106
6. Krenkel O, Tacke F. Liver macrophages in tissue homeostasis and disease. *Nat Rev Immunol* 2017, 17: 306–321
7. Tacke F, Luedde T, Trautwein C. Inflammatory pathways in liver homeostasis and liver injury. *Clinic Rev Allerg Immunol* 2009, 36: 4–12
8. Jiang J, Liu D, Wang Y, Li W, Hong Z, An J, Qiao S, *et al.* Glaucocalyxin a protect liver function via inhibiting platelet over-activation during sepsis. *Phytomedicine* 2022, 100: 154089
9. Xu W, Hou H, Yang W, Tang W, Sun L. Immunologic role of macrophages in sepsis-induced acute liver injury. *Int Immunopharmacol* 2024, 143: 113492
10. Shen L, Zhou T, Wang J, Sang X, Lan L, Luo L, Yin Z. Daphnetin reduces endotoxin lethality in mice and decreases LPS-induced inflammation in Raw264.7 cells via suppressing JAK/STATs activation and ROS production. *Inflamm Res* 2017, 66: 579–589
11. Loboda A, Damulewicz M, Pyza E, Jozkowicz A, Dulak J. Role of Nrf2/HO-1 system in development, oxidative stress response and diseases: an evolutionarily conserved mechanism. *Cell Mol Life Sci* 2016, 73: 3221–3247
12. Baird L, Dinkova-Kostova AT. The cytoprotective role of the Keap1–Nrf2 pathway. *Arch Toxicol* 2011, 85: 241–272
13. Baird L, Yamamoto M. Immunoediting of KEAP1-NRF2 mutant tumours is required to circumvent NRF2-mediated immune surveillance. *Redox Biol* 2023, 67: 102904
14. Liu F, Sun G, Gao H, Li R, Soromou LW, Chen N, Deng YH, *et al.* Angelicin regulates LPS-induced inflammation via inhibiting MAPK/NF-κB pathways. *J Surg Res* 2013, 185: 300–309
15. Yin Y, Mu F, Zhang L, Zhao J, Gong R, Yin Y, Zheng L, *et al.* Wedelolactone activates the PI3K/AKT/NRF2 and SLC7A11/GPX4 signalling pathways to alleviate oxidative stress and ferroptosis and improve sepsis-induced liver injury. *J EthnoPharmacol* 2025, 344: 119557
16. Matouk AI, El-Daly M, Habib HA, Senousy S, Naguib Abdel Hafez SM, Kasem ASW, Almalki WH, *et al.* Protective effects of menthol against sepsis-induced hepatic injury: role of mediators of hepatic inflammation,

apoptosis, and regeneration. *Front Pharmacol* 2022, 13: 952337
17. Crouser ED. Mitochondrial dysfunction in septic shock and multiple organ dysfunction syndrome. *Mitochondrion* 2004, 4: 729–741
18. Tepebaşi MY, Aşci H, Selçuk E, Kolay Ö, Milletsever A, Şahin M, Özmen Ö. Investigation of the theranekron ameliorative effect on sepsis-induced hepatotoxicity via inflammation and oxidative stress pathways. *Cell Biochem Biophys* 2025, 83: 3165–3175
19. Morgan MJ, Liu Z. Crosstalk of reactive oxygen species and NF-κB signaling. *Cell Res* 2011, 21: 103–115
20. Hommes DW, Peppelenbosch MP, van Deventer SJH. Mitogen activated protein (MAP) kinase signal transduction pathways and novel anti-inflammatory targets. *Gut* 2003, 52: 144–151
21. Fang H, Zhang Y, Wang J, Li L, An S, Huang Q, Chen Z, *et al.* Remimazolam reduces sepsis-associated acute liver injury by activation of peripheral benzodiazepine receptors and p38 inhibition of macrophages. *Int Immunopharmacol* 2021, 101: 108331
22. Hsu JT, Le PH, Lin CJ, Chen TH, Kuo CJ, Chiang KC, Yeh TS. Mechanism of salutary effects of melatonin-mediated liver protection after trauma-hemorrhage: P38 MAPK-dependent iNOS/HIF-1α pathway. *Am J Physiol Gastrointestinal Liver Physiol* 2017, 312: G427–G433
23. Wang Y, Ye L, Yan R, Zhou H, Zhao G. Ilex asprella polysaccharides alleviate liver injury via antioxidative, anti-inflammatory, and gut microbiota modulating effect. *Int J Biol Macromol* 2025, 306: 142024
24. Dai C, Zhang X, Lin J, Shen J. Nootkatone supplementation ameliorates carbon tetrachloride-induced acute liver injury via the inhibition of oxidative stress, NF-κB pathways, and the activation of Nrf2/HO-1 pathway. *Antioxidants* 2023, 12: 194
25. Wang L, He C. Nrf2-mediated anti-inflammatory polarization of macrophages as therapeutic targets for osteoarthritis. *Front Immunol* 2022, 13: 967193
26. Beyer D, Hoff J, Sommerfeld O, Zipprich A, Gaßler N, Press AT. The liver in sepsis: molecular mechanism of liver failure and their potential for clinical translation. *Mol Med* 2022, 28: 84
27. Huang K, Wu B, Hou Z, Ahmad A, Ahmed M, Khan AA, Tian F, *et al.* Psoralen downregulates osteoarthritis chondrocyte inflammation via an estrogen-like effect and attenuates osteoarthritis. *Aging* 2022, 14: 6716–6726
28. Li S, Li Q, Chen W, Zhong Y, Sun J, Wu J, Cao Y, *et al.* Psoralen attenuates cigarette smoke extract-induced inflammation by modulating CD8+ T lymphocyte recruitment and chemokines via the JAK2/STAT1 signaling pathway. *Heliyon* 2024, 10: e32351
29. Li X, Yu C, Hu Y, Xia X, Liao Y, Zhang J, Chen H, *et al.* New application of psoralen and angelicin on periodontitis with anti-bacterial, anti-inflammatory, and osteogenesis effects. *Front Cell Infect Microbiol* 2018, 8: 178
30. Liu X, Ou X, Zhang T, Li X, Qiao Q, Jia L, Xu Z, *et al.* In situ neutrophil apoptosis and macrophage efferocytosis mediated by Glycyrrhiza protein nanoparticles for acute inflammation therapy. *J Control Release* 2024, 369: 215–230
31. Prauchner CA. Oxidative stress in sepsis: pathophysiological implications justifying antioxidant co-therapy. *Burns* 2017, 43: 471–485
32. Liu X, Liao Y, Shao J, He D, Fan Z, Xu YN, Li C, *et al.* Angelicin improves osteoporosis in ovariectomized rats by reducing ROS production in osteoclasts through regulation of the KAT6A/Nrf2 signalling pathway. *Chin Med* 2024, 19: 91
33. Gao J, Zhao F, Yi S, Li S, Zhu A, Tang Y, Li A. Protective role of crocin against sepsis-induced injury in the liver, kidney and lungs via inhibition of p38 MAPK/NF-κB and Bax/Bcl-2 signalling pathways. *Pharm Biol* 2022, 60: 543–552
34. Li L, Eun JS, Nepal M, Ryu JH, Cho HK, Choi BY, Soh YJ. Isopsoralen induces differentiation of prechondrogenic ATDC5 cells via activation of MAP kinases and BMP-2 signaling pathways. *Biomolecules Ther* 2012, 20: 299–305
35. Gao N, Chen J, Li Y, Ding Y, Han Z, Xu H, Qiao H. The CYP2E1 inhibitor Q11 ameliorates LPS-induced sepsis in mice by suppressing oxidative stress and NLRP3 activation. *Biochem Pharmacol* 2023, 214: 115638
36. Warren GW, van Ess PJ, Watson AM, Mattson MP, Blouin RA. Cytochrome P450 and antioxidant activity in interleukin-6 knockout mice after induction of the acute-phase response. *J Interferon Cytokine Res* 2001, 21: 821–826
37. Abdulla D, Goralski K, Renton K. The regulation of cytochrome P450 2E1 during LPS-induced inflammation in the rat. *Toxicol Appl Pharmacol* 2006, 216: 1–10
38. Suo J, Zhang C, Wang P, Hou L, Wang Q, Zhao X. Allyl sulfide counteracts 1-bromopropane-induced neurotoxicity by inhibiting neuroinflammation and oxidative stress. *Toxicol Sci* 2019, 167: 397–407
39. Song BJ, Akbar M, Abdelmegeed MA, Byun K, Lee B, Yoon SK, Hardwick JP. Mitochondrial dysfunction and tissue injury by alcohol, high fat, nonalcoholic substances and pathological conditions through post-translational protein modifications. *Redox Biol* 2014, 3: 109–123
40. Lu Y, Cederbaum AI. Enhancement by pyrazole of lipopolysaccharide-induced liver injury in mice: role of cytochrome P450 2E1 and 2A5. *Hepatology* 2006, 44: 263–274
41. Tang C, Gao J, Li S, Cheng H, Peng YY, Ding Y, Yang H, *et al.* Chlorogenic acid improves SPS-induced PTSD-like behaviors in rats by regulating the crosstalk between Nrf2 and NF-κB signaling pathway. *Free Radical Biol Med* 2025, 231: 136–152
42. Yu M, Li H, Liu Q, Liu F, Tang L, Li C, Yuan Y, *et al.* Nuclear factor p65 interacts with Keap1 to repress the Nrf2-ARE pathway. *Cell Signal* 2011, 23: 883–892